Electronic Supplementary Material (ESI) for Chemical Communications.

Microswimming by Oxidation of Bibenzylamine

Martin Wittmann[1], Sandra Heckel[1], Felix Wurl[2], Zuyao Xiao[1], Thomas Gemming[3], Thomas Strassner[2] and Juliane Simmchen[1]

[1]Freigeist group, Physical Chemistry TU Dresden, Zellescher Weg 19, 01062 Dresden, Germany. E-mail: juliane.simmchen@tu-dresden.de

[2]Physical Organic Chemistry, Technische Universität Dresden,01069 Dresden, Germany.

[3]Leibniz Institute for Solid State and Materials Research Dresden, Helmholtzstraße 20, 01069 Dresden, Germany

March 3, 2022

Supporting Video: Different concentrations of DBA in ACN at 16 $\frac{\mathrm{W}}{\mathrm{cm}^2}$.

S1 Experimental Details

$BiVO_4$ particles were synthesised by a hydrothermal reaction. First $Bi(NO_3)_3 \cdot 5\,H_2O$ (5 mmol, 2.4245 g) was dissolved in 20 mL 2 M HNO_3, before NH_4VO_3 (5 mmol, 0.5849 g) was added under stirring leading to a yellow solution. The pH was adjusted to pH 2 using NH_3 and NaCl was added to a concentration of 0.05 M and sodium dodecyl sulfate (SDS) to a concentration of 0.005 M. After 15 min of stirring, the solution was transferred to a teflon lined autoclave and aged for 2 h followed by a hydrothermal treatment at 200 °C for 24 h. Finally

the obtained solution was washed three times with MilliQ water.

Microscopy experiments were carried out on an inverted Zeiss microscope. 25 µL of an acetonitrile solution containing the desired concentration of DBA and 0.1 $\frac{\text{mg}}{\text{mL}}$ $BiVO_4$ particles was placed on a plasma cleaned glass slide with an imaging spacer (diameter: 9 mm, height: 0.12 mm) and covered with a second glass slide. The $BiVO_4$ particles have a density, that is significantly larger than water and ACN, therefore they quickly sink to the bottom and swimm in 2D trajectories parallel to the substrate, which facilitates video recording. The particles were irradiated with a Colibri 7 light source and blue light: 469 nm and 0.4 $\frac{\text{W}}{\text{cm}^2}$ or 16 $\frac{\text{W}}{\text{cm}^2}$ from below and videos were recorded with 40 frames per second for 400 frames or more. Video analysis was performed with ImageJ 1.52e software and videos were tracked with the TrackMate plugin.[1] The resulting track files were processed with MATLAB R2018b.

The photocatalytic oxidation of DBA to *N*-Benzylidenebenzylamine was carried out in a quartz cuvette in a ACN solution containing 2.5 $\frac{\text{mg}}{\text{mL}}$ $BiVO_4$ and 20 $\frac{\text{mg}}{\text{mL}}$ DBA. We performed this experiment under different illumination conditions: For the Imine / Amine comparison in Figure 2, the solution was irradiated with a Opsytec solo P UV LED for 6 h, aliquots of 150 µL were taken after time steps of 1 h.

To compare the effect of stirring, we irradiated the samples using the Colibri lamp at 100% intensity for both, blue and UV light of 469 and 385 nm, respectively. The concentrations were identical to the experiment given above, only the sample volumes were reduced to 100 µL to enable longer sampling periods. Results are shown in Figure S1 and it becomes apparent, that stirring is still the better form of mixing. However, optimization of the micromotor geometry for efficient mixing was not the objective of this investigation.

In all above described cases, the aliquots were analysed by Gas chromatography coupled to a flame ionization detector (GC FID), Agilent 7890A gas chromatograph equipped with an Agilent HP-5 column and an Agilent 5975 Series mass-selective detector.

GC-FID measurements were carried out on an Agilent 6850 Series II gas chromatograph equipped with an Agilent HP-1 column and a flame ionization detector.

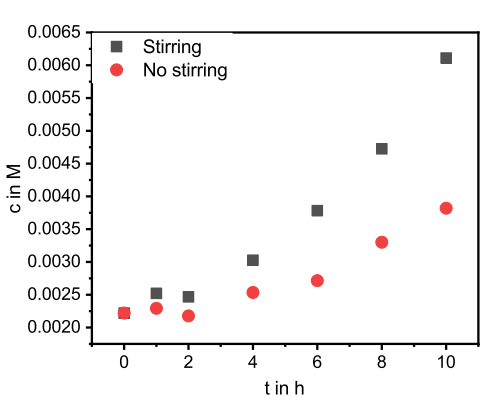

(A)

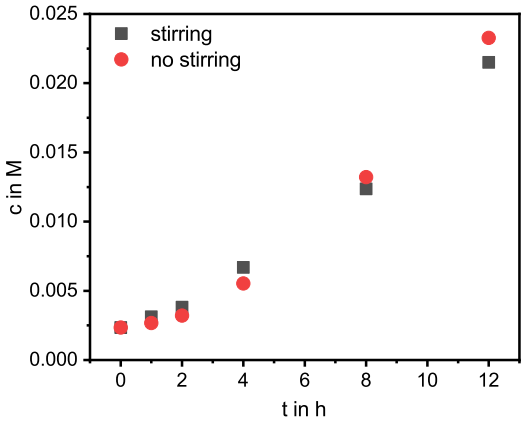

(B)

Figure S1: (A) Comparison of stirred and non stirred reaction in blue light of 469 nm with a light power of $\tilde{2}05$ mW. (B) Comparison of stirred and non stirred reaction in blue light of 385 nm with a light power of $\tilde{3}92$ mW.

XRD Measurements were carried out with a Bruker D2 phaser with Cu Kα radiation in Bragg Brentano geometry using a 2Θ range of 15-100 °. To analyze the optical properties of the materials DRS measurements were applied. Samples were prepared in a quarz cuvette in water. Measurements were carried out using a Cary 60 spectrophotometer with an integrating sphere (Agilent Technologies).

S2 Description to Figure 2 in main text

Figure 2A displays box plots of the speeds of $BiVO_4$ particles in ACN with DBA concentrations between 0.05 M and 1 M and two different light intensities. A clear trend to higher speeds with increasing DBA concentration can be observed: a combination of a low DBA concentration of 0.05 M and a light intensity of 0.4 $\frac{\mathrm{W}}{\mathrm{cm}^2}$ leads to motion with an average speed of just 4.2 $\frac{\mu\mathrm{m}}{\mathrm{s}}$, increasing steadily with both, fuel and illumination with a maximum mean value of 8.2 $\frac{\mu\mathrm{m}}{\mathrm{s}}$ at 1 M and $\frac{\mathrm{W}}{\mathrm{cm}^2}$. Analysis of the mean squared displacement (MSD) in a double logarithmic plot revealed presence of Brownian motion with a slope of $n = 1.1$ in ACN without DBA and ballistic motion with $n = 1.9$ in 1 M DBA solution (Figure 2B). All MSD plots and the corresponding slopes are given in Figure S3.

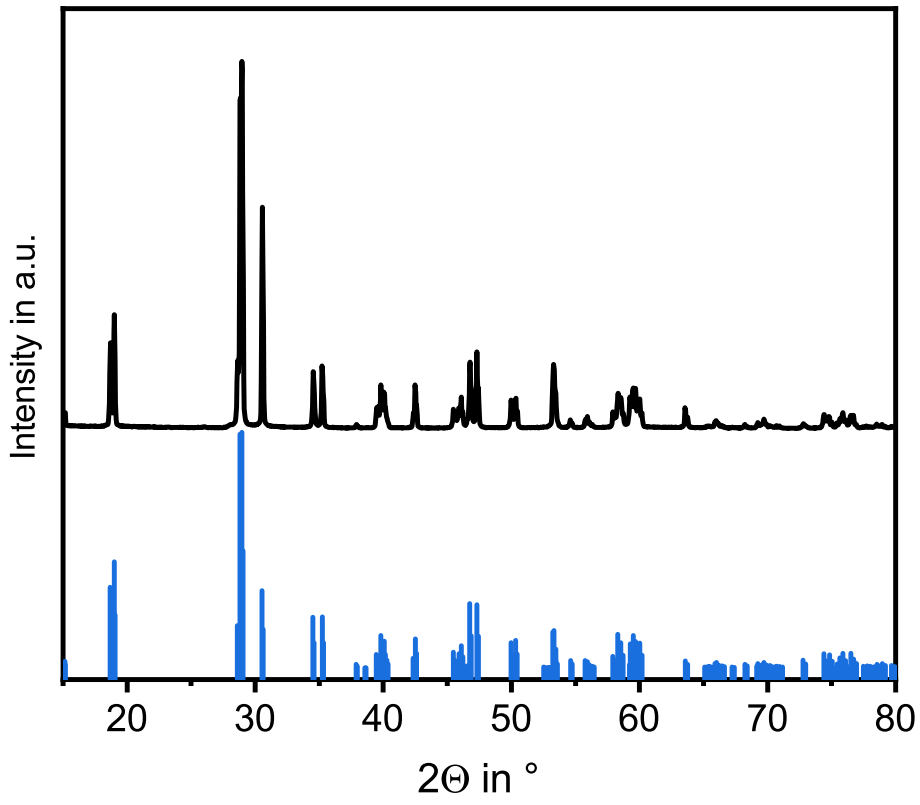

Figure S2: XRD of $BiVO_4$ particles.

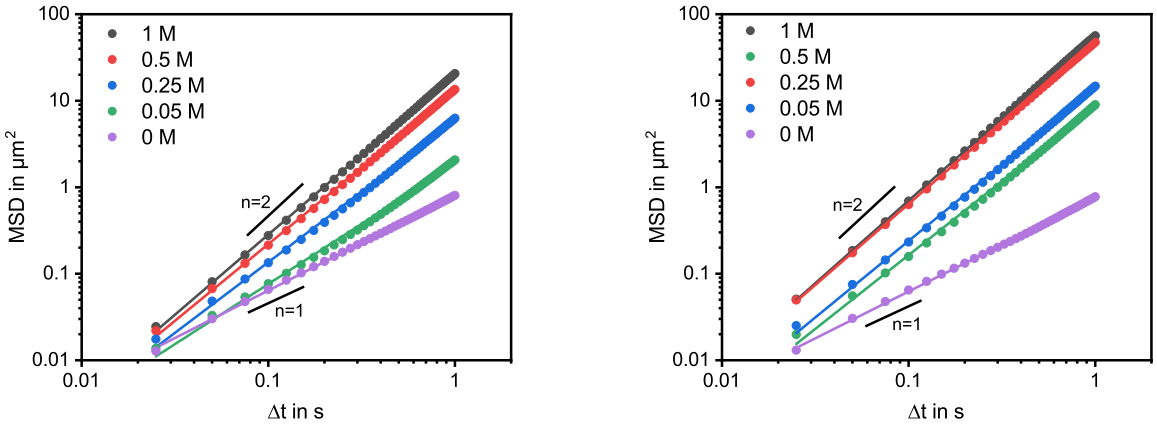

(A) (B)

Figure S3: Averaged double logarithmic MSD plots of particles in ACN with and without DBA under irradiation with blue light (A): 0.4 $\frac{W}{cm^2}$ and (B): 16 $\frac{W}{cm^2}$.

Table S1: Slopes n of linear fits of double logarithmic MSD plots with different DBA concentrations under irradiation with blue light with two intensities.

c(DBA) in M	0.4 $\frac{\mathrm{W}}{\mathrm{cm}^2}$	16 $\frac{\mathrm{W}}{\mathrm{cm}^2}$
0	1.1	1.1
0.05	1.4	1.7
0.25	1.6	1.8
0.5	1.8	1.9
1	1.9	1.9

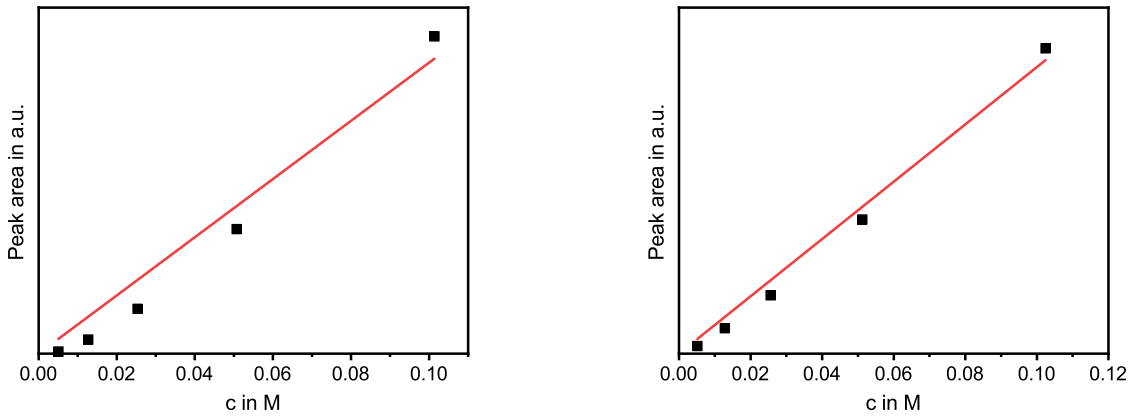

(A) (B)

Figure S4: Calibrations of (A): DBA and (B): *N*-Benzylidenebenzylamine at concentrations between 0.005 M and 0.1 M.

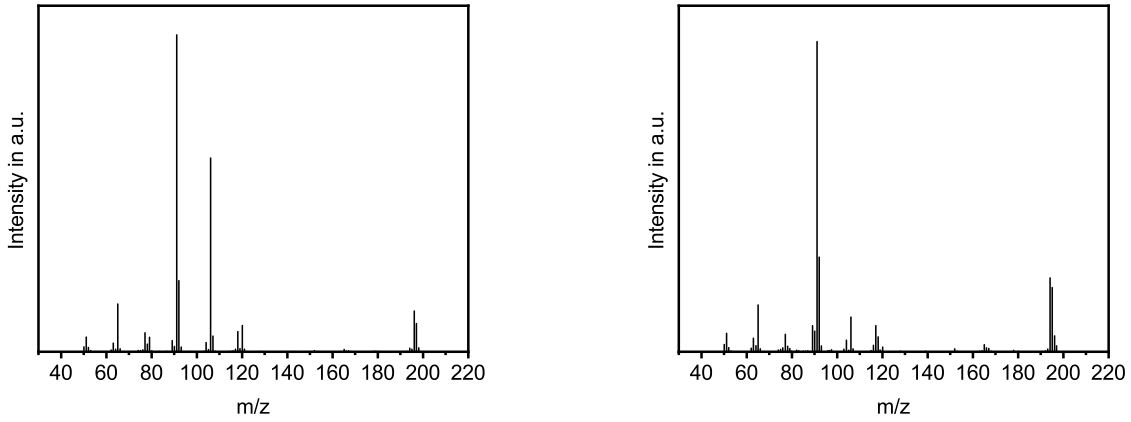

(A) (B)

Figure S5: Mass spectra of (A): DBA and (B): *N*-Benzylidenebenzylamine.

S3 Determination of power consumption

The efficiency is defined as

$$\eta = \frac{P_{output}}{P_{input}} = \frac{P_{mech}}{P_{chem}} \tag{S1}$$

The **power input** by the chemical reaction (P_{chem}) is given by Equation S2, where $k_{particle}$ stands for the reaction rate on one particle and ΔG_{free} for the free Gibb's energy. $k_{particle}$ is determined using the total reaction rate k_{total} (Equation S3), which we extract from the GC results.

$$P_{chem} = k_{particle} \cdot \Delta G_{free} \tag{S2}$$

$$k_{total} = \frac{\mathrm{d}c}{\mathrm{d}t} = 1.74 \times 10^{-6} \, \frac{\mathrm{mol}}{\mathrm{L\,s}} \tag{S3}$$

$k_{particle}$ can be calculated by dividing k_{total} by the number density $n_{particle}$ (Equation S4), which is defined as number of particles $N_{particle}$ per volume of solution $V_{solution}$ (Equation S5).

$$k_{particle} = \frac{k_{total}}{n_{particle}} \tag{S4}$$

$$n_{particle} = \frac{N_{particle}}{V_{solution}} \tag{S5}$$

The number density can be determined using the mass concentration of $BiVO_4$ in the solution β_{BiVO_4} (Equation S6), which has a value of 2.5 $\frac{\mathrm{mg}}{\mathrm{mL}}$. m_{BiVO_4} stands for the total mass of $BiVO_4$ in the solution and its ratio to the mass of a single particle ($m_{particle}$) corresponds to the total number of particles $N_{particle}$ (Equation S7).

$$\beta_{BiVO_4} = \frac{m_{BiVO_4}}{V_{solution}} = 2.5 \, \frac{\mathrm{mg}}{\mathrm{mL}} \tag{S6}$$

$$N_{particle} = \frac{m_{BiVO_4}}{m_{particle}} \tag{S7}$$

Equations S5,S6 and S7 result in Equation S8.

$$n_{particle} = \frac{\beta_{BiVO_4}}{m_{particle}} \tag{S8}$$

$m_{particle}$ is calculated by the average dimensions of the used $BiVO_4$ micro crystals and a density ρ of $6.9\,\frac{\mathrm{g}}{\mathrm{cm}^3}$ (from crystallographic data[2]). The truncated bipyramidal morphology is approximated by a cuboid with edge lengths of $a = b = 3.3\,\mu\mathrm{m}$ and $c = 1.4\,\mu\mathrm{m}$ (Equation S9.

$$m_{particle} = a \cdot b \cdot c \cdot \rho = 1.05 \times 10^{-13}\,\mathrm{kg} \tag{S9}$$

$$k_{particle} = \frac{k_{total} \cdot m_{particle}}{\beta_{BiVO_4}} = 7.32 \times 10^{-17}\,\frac{\mathrm{mol}}{\mathrm{particle\,s}} \tag{S10}$$

S3.1 Calculation of Free energies

All quantum chemical calculations were carried out with the Gaussian16 software package Revision A.03[3] employing the density functional model PBE[4,5]. The functional was combined with a DEF2QZVPP basis set[6,7,8] and the influence of the solvent described using the CPCM model[9,10] with acetonitrile as solvent. All given structures were verified as true minima by vibrational frequency analysis and the absence of negative eigenvalues. The approximate free energies were calculated from the thermochemistry data. Thermal corrections to the Gibbs free energy, as reported by Gaussian16, were considered including zero-point vibrations, thermal enthalpy corrections and entropy. All presented energies are free Gibbs energies at standard conditions (T=298.15 K, p=101.325 kPa) using unscaled frequencies. Geometries were visualised with GaussView6.0.[11]

The Gibbs free energy ΔG_{free} for the overall reaction of the amine oxidation (Figure S6) is calculated at $-193.3\,\mathrm{kJ/mol}$ per mole amin. The coordinates of the optimised geometries are

given below.

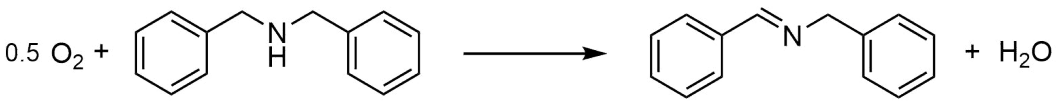

Figure S6: Overall reaction scheme of the amine oxidation for the calculation of the Gibbs free energy.

Table S2: Cartesian coordinates of O_2

atom	x	y	z
O	0.00000	0.00000	0.60893
O	0.00000	0.00000	-0.60893

Table S3: Cartesian coordinates of dibenzylamine.

atom	x	y	z
N	0.08433	-0.86344	1.00090
H	0.68581	-1.40285	1.62539
C	-1.25226	-1.47008	0.99004
H	-1.27756	-2.42981	0.43456
H	-1.50935	-1.70130	2.03536
C	0.70394	-0.82091	-0.33153
H	0.06395	-0.19454	-0.97305
H	0.74538	-1.82350	-0.80440
C	2.09469	-0.23760	-0.27036
C	3.22185	-1.05323	-0.43378
C	2.28541	1.13200	-0.03028
C	4.51160	-0.51706	-0.36225
H	3.08634	-2.12000	-0.62354
C	3.57034	1.67194	0.04129
H	1.41488	1.77795	0.09782
C	4.68857	0.84743	-0.12421
H	5.37779	-1.16654	-0.49381
H	3.70169	2.73944	0.22248
H	5.69273	1.26912	-0.07049
C	-2.30851	-0.54975	0.41135
C	-3.16602	-0.99160	-0.60381
C	-2.46540	0.75604	0.90056
C	-4.16195	-0.15514	-1.11814
H	-3.05040	-2.00366	-0.99759
C	-3.45579	1.59556	0.38873
H	-1.79748	1.11266	1.68612
C	-4.30927	1.14210	-0.62315
H	-4.81864	-0.51666	-1.91038
H	-3.56576	2.60724	0.78163
H	-5.08289	1.79824	-1.02329

Table S4: Cartesian coordinates of *N*-benzylidenebenzylamine.

atom	x	y	z
N	0.00448	-0.09232	0.98321
C	-0.98614	-0.81625	0.61836
H	-0.91576	-1.92145	0.60704
C	1.23131	-0.78065	1.37716
H	1.12236	-1.88012	1.31716
H	1.43623	-0.51833	2.42716
C	-2.28135	-0.26671	0.19276
C	-3.30516	-1.15606	-0.17483
C	-2.52886	1.11748	0.14119
C	-4.55026	-0.67721	-0.58499
H	-3.11760	-2.23086	-0.13656
C	-3.77072	1.59374	-0.26849
H	-1.73388	1.80645	0.42598
C	-4.78545	0.69874	-0.63262
H	-5.33662	-1.37736	-0.86752
H	-3.95458	2.66788	-0.30620
H	-5.75685	1.07645	-0.95274
C	2.39927	-0.33081	0.52198
C	3.18590	0.76649	0.89665
C	2.69379	-0.99455	-0.67667
C	4.24478	1.19311	0.09119
H	2.96935	1.28798	1.83097
C	3.75281	-0.57272	-1.48408
H	2.09004	-1.85312	-0.97757
C	4.53055	0.52409	-1.10210
H	4.85067	2.04643	0.39796
H	3.97330	-1.10309	-2.41115
H	5.35904	0.85321	-1.72996

Table S5: Cartesian coordinates of H_2O.

atom	x	y	z
O	0.00000	0.00000	0.11981
H	0.00000	0.76278	-0.47924
H	0.00000	-0.76278	-0.47924

S4 Determination of power output

The **power output** was determined using Equation S11, where v refers to the particle speed and F_{drag} for the drag force.

$$P_{mech} = F_{drag} \cdot v = f \cdot v^2 \tag{S11}$$

F_{drag} was determined using the approach by Leith (Equation S12) with a dynamic shape factor K as defined in Equation S13. There, μ stands for the dynamic viscosity of the solution (0.343 mPa s) and d_v, d_n and d_s stand for the diameter of a sphere with: the same volume as the particle (d_v), the same surface area as the particle (d_s) and the same projected area in direction of motion as the particle (d_n).

$$F_{drag} = 3\pi \cdot \mu \cdot v \cdot d_v \cdot K \tag{S12}$$

$$K = \frac{1}{3} \cdot \frac{d_n}{d_v} + \frac{2}{3} \cdot \frac{d_s}{d_v} \tag{S13}$$

S4.1 Finite element simulation

The model was implemented in the COMSOL Multiphysics package (version 5.6) with a 2D configuration to simulate the electrophoresis of $BiVO_4$ particles. In this model, a truncated pyramid of 1.4 µm in height and 3.3 µm in length is placed above a substrate with a separation distance of 300 nm and in the center of a cube box with a length of 100 µm. The cube is set to be a calculated domain and fulfilled with ACN. The distribution of electric field and fluid flow field of the domain is solved with a nonlinear steady solver built in COMSOL.

In this self-electrophoresis model, the oxidation of DBA and reduction of oxygen occur preferentially at the {110} and {010} face respectively. According to the GC - MS measurement, the outward flux at the anode was set to be 6.72×10^{-6} $\frac{\text{mol}}{\text{m}^2\,\text{s}}$, while the inward flux at the cathode is set to be 6.4×10^{-6} $\frac{\text{mol}}{\text{m}^2\,\text{s}}$ to ensure mass conservation.

In the electrostatic module, the calculated domain is governed by the following equation (Equation S14):

$$E = -\nabla V \tag{S14}$$

where E is electric field in space and V is electric potential. E is further solved by the space charge density at each point in the domain by (Equation S15):

$$\nabla \cdot (\epsilon E) = \rho_V \tag{S15}$$

where ϵ is medium electrical permittivity and ρ_V is space charge density.

The anode face with an outward flux carries an extrinsic surface charge density ρ_a by (Equation S16)[13]:

$$\rho_a = \epsilon E_a = \epsilon \frac{J_a K_B T}{2 e n_0 D_{H+}} \tag{S16}$$

where ϵ is the medium electrical permittivity, n_0 is the bulk proton concentration, J_a is the ionic flux on anode.

The cathode with an inward flux carries an opposite surface charge density ρ_c by (Equation S17),

$$\rho_c = \epsilon E_c = \epsilon \frac{J_c K_B T}{2 e n_0 D_{H+}} \tag{S17}$$

where J_c is the flux on cathode.

In creeping flow module, the calculated domain is governed by the following equation:

$$\nabla \cdot u = 0 \tag{S18}$$

$$\nabla p = \eta \nabla^2 u \tag{S19}$$

where p is the pressure, η is the dynamic viscosity of water, and u is the fluid flow velocity.

The two modules are coupled by an electroosmotic boundary condition on the particle and substrate surface:

$$U_{eo} = \frac{\zeta\epsilon}{\eta} E_{tan} \tag{S20}$$

Where U_{eo} is the electroosmotic speed of the fluid on the particle and substrate surface, ζ is the zeta potential (particle set to be -20 mV, substrate set to be -50 mV), and E_{tan} is the tangential component of the electric field that is solved by the (Equation S14) and (Equation S15).

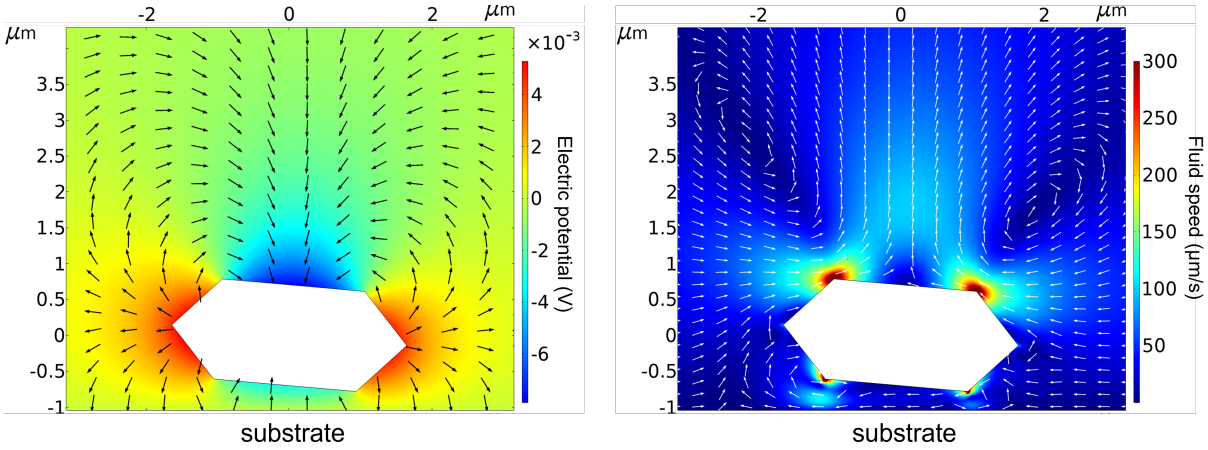

Figure S7: Simulation result of the electrophoresis of $BiVO_4$ particles. (A):Electric potential (color-coded) and electric field (black arrows) distribution around a $BiVO_4$ particle. (B):Fluid speed magnitude (color-coded) and flow field lines (white arrows) around a $BiVO_4$ particle.

Since the particle is fixed and on its own reference frame, we investigate the fluid speed near the cube edge to represent the particle's speed (1.14 µm/s). The drag force is obtained by integrating the fluid stress exerted over the particle surface (9.12×10^{-13} N).

S5 Hypothesis on the origin of asymmetry

The asymmetry of the micro crystals required for active motion originates from two different factors. Firstly, irradiation with blue light is performed from the bottom, which leads to a higher reaction rate on the bottom of the particle than on the top. If the particle is in an inclined orientation, this self shadowing can cause an asymmetric flow field in the surrounding fluid as shown in Figure S8 A and further described in[14]. Secondly, the reactivities of the individual facets differ because of synthetic surface defects as shown in the SEM images in Figure S8 B.

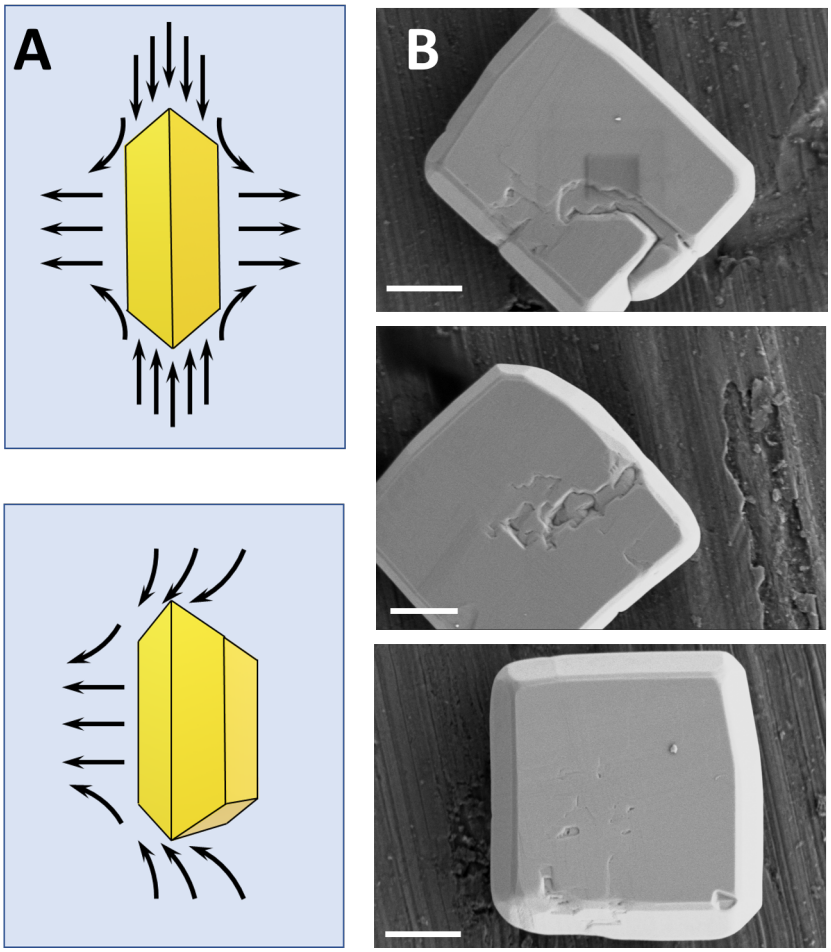

Figure S8: We assume the asymmetry to originate mostly from two factors: A) in the more active cases, a self-enhancing influence is obtained from the tilt of the particle (see also[14]). B) inhomogeneities and defects in the particle morphologies lead to intrinsic asymmetry (compare[15], scale bars correspond to 1 µm.)

References

[1] J.-Y. Tinevez, N. Perry, J. Schindelin, G. M. Hoopes, G. D. Reynolds, E. Laplantine, S. Y. Bednarek, S. L. Shorte and K. W. Eliceiri, *Methods*, 2017, **115**, 80–90.

[2] A. Sleight, H. y. Chen, A. Ferretti and D. Cox, *Materials Research Bulletin*, 1979, **14**, 1571–1581.

[3] M. J. Frisch, G. W. Trucks, H. B. Schlegel, G. E. Scuseria, M. A. Robb, J. R. Cheeseman, G. Scalmani, V. Barone, G. A. Petersson, H. Nakatsuji, X. Li, M. Caricato, A. V. Marenich, J. Bloino, B. G. Janesko, R. Gomperts, B. Mennucci, H. P. Hratchian, J. V. Ortiz, A. F. Izmaylov, J. L. Sonnenberg, D. Williams-Young, F. Ding, F. Lipparini, F. Egidi, J. Goings, B. Peng, A. Petrone, T. Henderson, D. Ranasinghe, V. G. Zakrzewski, J. Gao, N. Rega, G. Zheng, W. Liang, M. Hada, M. Ehara, K. Toyota, R. Fukuda, J. Hasegawa, M. Ishida, T. Nakajima, Y. Honda, O. Kitao, H. Nakai, T. Vreven, K. Throssell, J. A. Montgomery Jr., J. E. Peralta, F. Ogliaro, M. J. Bearpark, J. J. Heyd, E. N. Brothers, K. N. Kudin, V. N. Staroverov, T. A. Keith, R. Kobayashi, J. Normand, K. Raghavachari, A. P. Rendell, J. C. Burant, S. S. Iyengar, J. Tomasi, M. Cossi, J. M. Millam, M. Klene, C. Adamo, R. Cammi, J. W. Ochterski, R. L. Martin, K. Morokuma, O. Farkas, J. B. Foresman and D. J. Fox, *Gaussian 16, Revision A.03*, 2016, http://www.gaussian.com.

[4] J. P. Perdew, K. Burke and M. Ernzerhof, *Physical Review Letters*, 1996, **77**, 3865–3868.

[5] J. P. Perdew, K. Burke and M. Ernzerhof, *Physical Review Letters*, 1997, **78**, 1396.

[6] F. Weigend, F. Furche and R. Ahlrichs, *Journal of Chemical Physics*, 2003, **119**, 12753–12762.

[7] F. Weigend and R. Ahlrichs, *Physical Chemistry Chemical Physics*, 2005, **7**, 3297–3305.

[8] F. Weigend, *Physical Chemistry Chemical Physics*, 2006, **8**, 1057–1065.

[9] V. Barone and M. Cossi, *Journal of Physical Chemistry A*, 1998, **102**, 1995–2001.

[10] M. Cossi, N. Rega, G. Scalmani and V. Barone, *Journal of Computational Chemistry*, 2003, **24**, 669–681.

[11] R. Dennington, T. A. Keith and J. M. Millam, *GaussView, Version 6.0*, 2016.

[12] D. Leith, *Aerosol science and technology*, 1987, **6**, 153–161.

[13] T. R. Kline, J. Iwata, P. E. Lammert, T. E. Mallouk, A. Sen and D. Velegol, *The Journal of Physical Chemistry B*, 2006, **110**, 24513–24521.

[14] S. Heckel, C. Bilsing, M. Wittmann, T. Gemming, L. Büttner, J. Czarske and J. Simmchen, 2021.

[15] S. Heckel and J. Simmchen, *Advanced Intelligent Systems*, 2019, **1**, 1900093.